Scripta Materialia 129 (2017) 65–68

Contents lists available at ScienceDirect

Scripta Materialia

journal homepage: www.elsevier.com/locate/scriptamat

Regular Article

Novel TiNbTaZrMo high-entropy alloys for metallic biomaterials

Mitsuharu Todai [a], Takeshi Nagase [a,b], Takao Hori [a], Aira Matsugaki [a], Aiko Sekita [a], Takayoshi Nakano [a,*]

[a] Division of Materials and Manufacturing Science, Graduate School of Engineering, Osaka University, 2-1 Yamadaoka, Suita, Osaka 565-0871, Japan
[b] Research Center for Ultra-High Voltage Electron Microscopy, Osaka University, 7-1, Mihogaoka, Ibaraki, Osaka 567-0047, Japan

ARTICLE INFO

Article history:
Received 5 October 2016
Accepted 21 October 2016
Available online 9 November 2016

Keywords:
Biomaterials
High-entropy alloys (HEAs)
Microstructure
Solidification
Crystal structure

ABSTRACT

A novel equiatomic TiNbTaZrMo high-entropy alloy (HEA) was developed as a new metallic biomaterial. The constituent elements of the HEA were biocomparable, and the HEA was designed based on parameters such as the mixing enthalpy (ΔH_{mix}), the omega parameter (Ω), the delta parameter (δ), and the valence electron concentration (VEC) theory. The bcc solid solution phases with the different lattice constants were obtained in as-cast and annealed states. The HEA showed considerable strength with deformability and superior biocompatibility comparable to pure Ti. This study demonstrated the possibility of using HEAs as a new class of metallic biomaterials.

A wide variety of metallic biomaterials has been developed to date. However, there is a strong need for a new generation of metallic biomaterials with superior biocompatibility and mechanical properties to meet future demands of the medical field. Recently, a new class of structural materials, called high-entropy alloys (HEAs), has been developed [1–6]. These alloys consist of multicomponent elements with an approximately equiatomic ratio of various components for maximizing the configurational entropy, which stabilizes the solid solution phase. The complicated arrangement of different atomic species in HEAs is considered to give rise to a number of advantages over common and/or single-element-based alloys. These include the formation of a solid solution, which gives rise to deformability and a severely distorted lattice, which strengthens the material. HEAs may simultaneously realize superior mechanical properties and biocompatibility, which makes them suitable for use as a new class of metallic biomaterials. Among common metallic biomaterials, Ti-rich Ti–Nb–Ta–Zr (TNTZ) alloys with a bcc phase have been widely investigated as superior Ti-based metallic biomaterials. The constituent elements of these alloys are non-toxic and allergy-free [7–10]. The combination of Ti, Nb, Ta, and Zr is favorable for the formation of a single solid solution phase in alloys based on the alloy design of HEAs (see Section S1 in the Supplementary material). In the present study, a novel TiNbTaZrMo HEA was designed from an equiatomic TiNbTaZr alloy, and the microstructure and biocompatibility of the TiNbTaZrMo HEA was investigated in order to clarify the possible use of HEAs as a new class of metallic biomaterials.

Various parameters have been suggested for predicting the formation of solid solution phases in multicomponent alloys and for the development of HEAs. In the present study, the heat of mixing (ΔH_{mix}) [4–6,11,12], delta parameter (δ) (which determines the atomic-size difference in multicomponent alloys) [4–6,12–14], and omega parameter (Ω) (defined by the combination of ΔS_{mix}, ΔH_{mix}, and the melting temperatures of the constituent elements) [5,6,14] were used. The possibility of forming a solid solution and the structure of the resulting solid solution in the equiatomic TiNbTaZr and TiNbTaZrX (X = Cr, V, Mo, W, Fe) alloys is discussed. The element X in these alloys was selected from elements in which a bcc-structured phase is formed at room temperature. The stability of fcc and bcc solid solutions in HEAs can be predicted by the valence electron concentration (VEC) parameter [15]. The HEA parameters of the TiNbTaZr and TiNbTaZrX (X = Cr, V, Mo, W, Fe) alloys are summarized in Table 1, along with those of typical HEAs such as a refractory TiNbTaZrHf HEA [16,17] and CoCrMnFeNi HEA [1] as a reference. The parameters of the atomic radius and ΔH_{ij}, which is the mixing enthalpy of an A–B (i = A, j = B, i ≠ j) binary system at an equiatomic composition ($A_{50}B_{50}$) for a liquid phase, were taken from literature [11]. Zhang et al. showed that solid solutions are formed in the alloys satisfying the criteria $-20 \le \Delta H_{mix} \le 5$, $\delta \le 6.4$, and $12 \le \Delta S_{mix} \le 17.5$ [4]. Guo et al. suggested that the following conditions are favorable for the formation of solid solutions: $-11.6 \le \Delta H_{mix} \le 3.2$ and $\delta \le 6.6$ [12]. Yang et al. suggested that $\Omega \ge 1.1$ and $\delta \le 6.6$ should be used as necessary conditions to predict the formation of solid solution phases [14]. Although some inconsistencies are observed between the above-mentioned criteria, the criteria are helpful in predicting the formation of solid solution phases in multicomponent alloys. The VEC parameters in the TiNbTaZr and TiNbTaZrX (X = Cr, V, Mo, W, Fe) alloys were found to be <5.0, indicating the strong bcc structure formation tendency of these alloys when a solid solution phase is obtained. According to the above-mentioned criteria, TiNbTaZr and $TiNbTaZrX_1$ (X_1 = Mo, W) show a high possibility for the formation of a solid solution, whereas $TiNbTaZrX_2$ (X_2 = Cr, V, and Fe) alloys are

* Corresponding author.
E-mail address: nakano@mat.eng.osaka-u.ac.jp (T. Nakano).

http://dx.doi.org/10.1016/j.scriptamat.2016.10.028

Table 1
Alloy parameters of ΔS_{mix} [J/mol K], ΔH_{mix} [kJ/mol], δ [%], Ω, and VEC in the equiatomic TiNbTaZr and TiNbTaZrX (X = Cr, V, Mo, W, Fe) alloys. "R" in the ΔS_{mix} column is the gas constant.

Alloys	ΔS_{mix}	ΔH_{mix}	δ	Ω	VEC	Phase	References
TiNbTaZr	1.42R	2.5	5.3	11.6	4.50	bcc	Present study
TiNbTaZrMo	1.61R	−1.8	5.9	19.7	4.80	bcc1 + (bcc2)	Present study
TiNbTaZrW	1.61R	−3.2	5.8	11.5	4.80	bcc1 + (bcc2)	[18]
TiNbTaZrV	1.61R	0.3	6.7	101	4.60	bcc	[19]
TiNbTaZrCr	1.61R	−3.7	8.2	8.9	4.80	Compounds	[19]
TiNbTaZrFe	1.61R	−10.1	8.4	3.2	5.20		
TiNbTaZrHf	1.61R	2.7	5.5	12.4	4.40	bcc	[16,17]
CoCrMnFeNi	1.61R	3.2	1.1	7.4	8.80	fcc	[1]

not expected to show superior solid-solution-forming ability because of the large value of δ. Between W and Mo, Mo is preferred for the fabrication of metallic biomaterials because Mo has been selected in conventional metallic biomaterials such as Ti–15Mo–5Zr–3Al [20–22] and Co–Cr–Mo [23,24]. In the present study, the TiNbTaZr and TiNbTaZrMo alloys were newly focused, and the microstructure, mechanical properties and biocompatibility of TiNbTaZrMo were investigated in terms of using HEAs as a new class of metallic biomaterials.

Arc-melted ingots were prepared by mixing lumps of the pure elements. To achieve a homogeneous distribution of the constituent elements in the alloy, the alloy was melted >10 times and maintained in a liquid state for approximately 300 s during each melting event. The annealed samples were obtained by vacuum annealing at 1273 K for 168 h. The microstructure and constituent phases of the ingots were investigated by X-ray diffraction (XRD) analysis, optical microscopy (OM), scanning electron microscopy (SEM), electron probe microanalysis (EPMA), and transmission electron microscopy (TEM). Rectangular specimens for compression testing with dimensions of approximately 2 mm × 2 mm × 5 mm were cut from the ingots by electron discharge machine. Compression tests were conducted using an Intron-type testing machine at nominal strain rate of $1.67 \times 10^{-4}\ s^{-1}$ at room temperature. The specimens for the cell culture experiment to evaluate biocompatibility were cut into $\phi = 9$ mm × 1 mm using an electron discharge machine. The surface of these specimens were mechanically polished using SiC waterproof papers up to 4000 grit and a diamond paste. Prior to the cell culture experiment, these specimens were sterilized by ultraviolet (UV) light at room temperature and then placed individually into a 48-well plate ($n = 5$). Primary osteoblasts were isolated from neonatal mice calvariae by sequential collagenase/trypsin digestion. The obtained cells were diluted to 6000 cells/cm^2 and seeded onto the specimens. After culturing for 24 h in a 5% CO_2 humidified atmosphere, the cells were fixed with methanol and stained with a 5% Giemsa aqueous solution. The cell density was evaluated with OM images. Data are expressed as mean ± SD (standard deviation). Statistical significance was assessed using one-way ANOVA, followed by Tukey's post-hoc test. A significance of $P < 0.05$ was required for rejection of the null hypothesis. As a comparison, the biocompatibility of specimens made of conventional stainless steel (SUS 316L) and commercially pure Ti (CP-Ti) were evaluated by the same method used for the TiNbTaZrMo alloys.

Fig. 1 shows the microstructure analysis results of the TiNbTaZrMo alloy, together with the XRD pattern of a quaternary TiNbTaZr alloy as a reference. Fig. 1a shows the XRD patterns of the TiNbTaZr and TiNbTaZrMo alloys. The TiNbTaZr alloy shows sharp diffraction peaks, indicated by the index ●, and all peaks were identified as a bcc solid solution phase. The lattice constant of the bcc phase in the TiNbTaZr alloy evaluated by XRD was 0.332 nm, which is in good agreement with that estimated by the linear combination of pure elements (i.e., Vegard's law [25], 0.336 nm). From the XRD pattern of the TiNbTaZrMo alloy, the two peaks indicated by the indexes ● and ○ can be seen in the as-cast state. The constituent phases in the as-cast TiNbTaZrMo alloy were identified as a main bcc solid solution phase

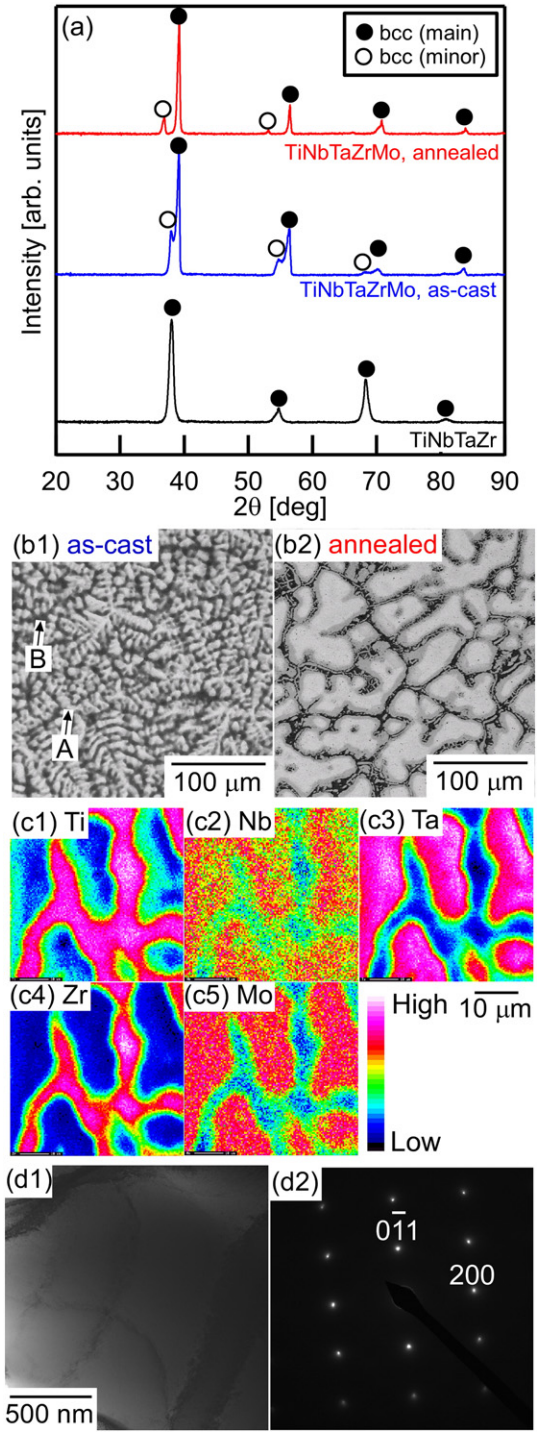

Fig. 1. Microstructure of the equiatomic TiNbTaZrMo HEAs as-cast and annealed at 1273 K for 168 h. (a) XRD patterns. (b1, b2) SEM-BSE images: (b1) as-cast state and (b2) annealed at 1273 K for 168 h. (c1–c5) EPMA elemental mapping results of as-cast sample: (c1) Ti image, (c2) Nb image, (c3) Ta image, (c4) Zr image, and (c5) Mo image. (d1, d2) TEM analysis results of as-cast sample: (d1) TEM-BF image and (d2) SAED pattern in [011] direction.

with a lattice constant of 0.325 nm (●) and a minor bcc phase with a lattice constant of 0.333 nm (○). The XRD patterns did not indicate the formation of any intermetallic compound phases or bcc-based ordered phases. These results suggest that the as-cast specimens for the TiNbTaZr and TiNbTaZrMo alloys had bcc solid solutions without any inclusions. The annealing did not lead the decomposition of bcc solid solution phases to other phases and the formation on intermetallic compounds in TiNbTaZrMo alloy, and stimulates the slight change in minor

bcc phase (●). The peak positions of the minor bcc phase were shifted to the low-angle side, and the peak intensity ratio of the minor bcc phase (●)/main bcc phase (○) decreased. These results indicate the formation of bcc HEA with high phase stability in the TiNbTaZrMo alloy. Fig. 2b1 and b2 shows the SEM-back scattering electron (BSE) image of the TiNbTaZrMo HEA. An equi-axis fine dendrite structure was observed in the as-cast TiNbTaZrMo HEA, and this was independent of the sample position in the ingots. A dendrite structure indicates the redistribution of the constituent elements during solidification, which results in the formation of a mixture of a main-dendrite phase with a white contrast (index A) and a minor phase of the inter-dendrite region with a dark-gray contrast (index B). As observed from the contrast in the SEM-BSE image (Fig. 2b1), the inter-dendrite region appeared to be a single phase. The coarsening of the main dendrite phase with white contrast can be seen in the annealed TiNbTaZrMo HEA (Fig. 2b2). Fig. 2c1–c5 shows the elemental mapping obtained using EPMA, focusing on the distribution of the constituent elements and chemical homogeneity in the main-dendrite (A) and inter-dendrite (B) regions in the as-cast TiNbTaZrMo HEA. The regions A and B both contained all the constituent elements, which led to the formation of multicomponent solid solution phases. The region A was enriched with Ta, Nb, and Mo, whereas Ti and Zr were concentrated in region B. The composition analysis results obtained by EPMA-wavelength dispersive X-ray spectroscopy (WDS) were as follows: in the region A, Ti 15.5 ± 0.4 [at%], Nb 22.4 ± 0.4 [at%], Ta 30.8 ± 0.8 [at%], Zr 8.4 ± 0.5 [at%], and Mo 22.9 ± 0.6 [at%]; whereas, in the region B, Ti 24.7 ± 0.2 [at%], Nb 13.6 ± 0.6 [at%], Ta 7.7 ± 0.5 [at%], Zr 40.9 ± 1.5 [at%], and Mo 13.1 ± 0.6 [at%]. The distribution of the constituent elements in the annealed TiNbTaZrMo HEA was similar to those in the as-cast specimens. The lattice constants estimated by Vegard's law and the WDS analysis results of the A and B phases in the as-cast TiNbTaZrMo HEA were 0.328 and 0.338 nm, respectively, and these values are similar to those evaluated by XRD analysis (Fig. 1). Fig. 2d1 and d2 shows the TEM-bright-field (BF) image and the corresponding selected area electron diffraction (SAED) pattern, respectively, along the [011] direction obtained from the main-dendrite phase in the as-cast specimens. No crystalline precipitates in main bcc phase were observed from the TEM-BF image (Fig. 2d1). The SAED pattern showed no minor peaks corresponding to the ω phase or to ordered phases such as the B2 structure (Fig. 2d2). These results indicate the formation of a bcc solid solution phase without a significant chemically ordered structure or inclusions in the as-cast TiNbTaZrMo HEA. The distribution of the constituent elements during solidification led to the formation of the equiatomic dendrite structure, which then resulted in the formation of a Ta-, Mo-, and Nb-rich main-dendrite phase (A) and a Ti- and Zr-rich minor bcc phase in the inter-dendrite region (B) in the as-cast specimens. The distribution of the constituent elements in the TiNbTaZrMo HEA can be qualitatively explained in terms of ΔH_{ij} without any discrepancy as follows: during the solidification, the main-dendrite phase with high-melting-temperature elements (Ta, Mo, and Nb) was formed. Ti and Zr were ejected from the dendrite phase because of the positive values of $\Delta H_{Ta\ Ti}$, $\Delta H_{Ta\ Zr}$, $\Delta H_{Nb\ Ti}$, and $\Delta H_{Nb\ Zr}$ [11], resulting in the enrichment of the inter-dendrite region with Ti and Zr. The high solid-solution-forming ability of the alloys with Ti, Nb, Ta, Zr, and Mo led to the formation of HEAs with a bcc structure composed of equi-axis dendrites.

The room-temperature engineering stress vs. plastic strain curves of the TiNbTaZrMo HEAs in the as-cast and annealed states obtained during compression testing are given in Fig. 2. The inset shows the 0.2% proof stress ($\sigma_{0.2}$) of the TiNbTaZrMo HEAs in the as-cast and annealed states, together with those of refractory TiNbTaZrHf HEA [16,17] and Ti–6Al–4V [26] as references. The as-cast and annealed TiNbTaZrMo HEAs show a high $\sigma_{0.2}$ of >1000 MPa. The values of $\sigma_{0.2}$ in the TiNbTaZrMo HEAs are higher than those of the refractory TiNbTaZrHf HEA and Ti–6Al–4V alloys. The annealing was effective in improving the deformability of the TiNbTaZrMo HEA, which may be related to the grain coarsening and/or redistribution of the constituent elements in the main-dendrite and inter-dendrite regions. The TiNbTaZrMo HEA shows high yield strength and good deformability.

Fig. 3 shows the osteoblasts cultured for 24 h on SUS316L (Fig. 3a), CP-Ti (Fig. 3b), and TiNbTaZrMo HEA in the as-cast (Fig. 3c) and annealed (Fig. 3d) states. The osteoblasts on the surfaces of the as-cast and annealed TiNbTaZrMo HEAs show a widespread morphology, which is quite similar to the morphology of the cells on CP-Ti. In

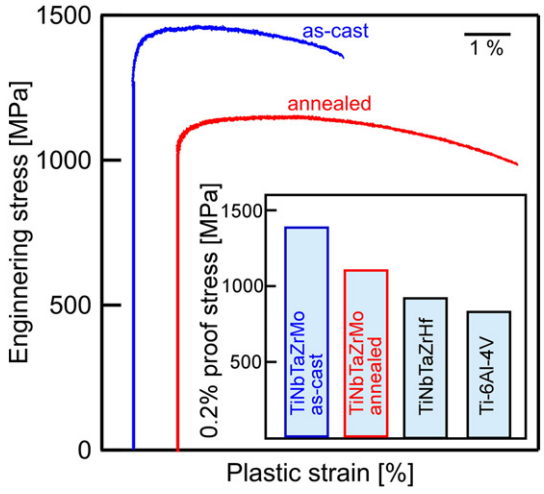

Fig. 2. Engineering stress vs. plastic strain compression curves of the equiatomic TiNbTaZrMo HEAs as cast and annealed at 1273 K for 168 h.

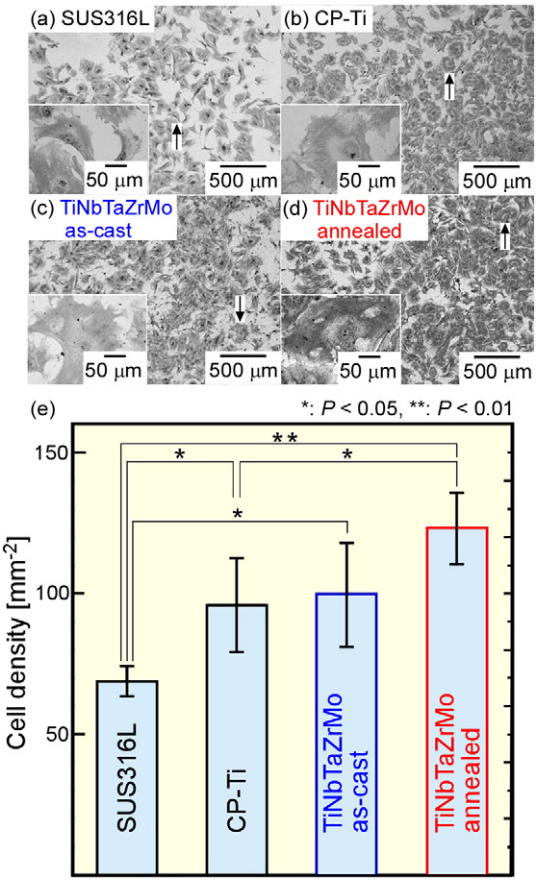

Fig. 3. Giemsa staining of the osteoblasts cultured on (a) SUS316L, (b) CP-Ti, (c) as-cast TiNbTaZrMo, and (d) TiNbTaZrMo HEA annealed at 1273 K for 168 h. The insets show the magnified images of the cells indicated as black arrows. (e) Quantitative analysis of cell density after 24 h cultivation on each alloy.

contrast, the osteoblasts on SUS316L show a relatively small, less widespread morphology. Cell spreading plays a significant role in cellular functions involving migration, proliferation, and protein synthesis. The obtained results indicate that the osteoblasts on the TiNbTaZrMo HEAs with and without annealing, as well as on CP-Ti, have a significant advantage in bone matrix formation. The cell density analyzed after 24 h cultivation quantitatively revealed that the osteoblasts on the as-cast and annealed TiNbTaZrMo HEAs had a significantly increased number of cells as compared to SUS316L. Notably, the as-cast TiNbTaZrMo HEA showed excellent biocompatibility comparable to that of CP-Ti. Moreover, the significantly superior biocompatibility of the annealed TiNbTaZrMo HEA as compared to CP-Ti is demonstrated for the first time (Fig. 3e). This indicates that the grain coarsening and/or redistribution of the constituent elements in the annealed TiNbTaZrMo HEA possibly accelerated the osteoblast adhesion. The combination of a Ti oxide layer and a Zr oxide layer in a TNTZ alloy has been shown to exhibit excellent biocompatibility [27]. Furthermore, a Ti–30Zr–7Mo alloy was reported to have shown a significantly increased number of cells as compared to CP-Ti, allowing the formation of a Zr oxide layer, as well as a Ti oxide layer [28]. Taken together, the excellent biocompatibility in the TiNbTaZrMo HEA obtained in this study may be due to the particular oxide layer based on the complicated arrangement of constituent metallic elements. Further research is necessary for clarifying the origin of the excellent biocompatibility in the TiNbTaZrMo HEA, which will be reported in future works. These results clearly indicate that the HEA shows potential as a new class of metallic biomaterials.

In conclusion, a novel equiatomic TiNbTaZrMo HEA composed of biocomparable elements was successfully developed as a metallic biomaterial. Two bcc solid solution phases were obtained in the TiNbTaZrMo HEA. An equi-axis fine dendrite structure was observed in the ingots. The HEA showed excellent biocompatibility compared to that of pure Ti, together with superior mechanical properties, indicating the possibility of using HEAs as a new class of metallic biomaterials.

Acknowledgements

This work was partially supported by JSPS KAKENHI (grant number 25220912), the Council for Science, Technology and Innovation (CSTI), Cross-Ministerial Strategic Innovation Promotion Program (SIP), Innovative design/manufacturing technologies (Establishment and Validation of the base for 3D Design & Additive Manufacturing Standing on the Concepts of “Anisotropy” & “Customization”) of the New Energy and Industrial Technology Development Organization (NEDO), and by scientific grants from the Japan Foundry Engineering Society (JFS).

Appendix A. Supplementary data

Supplementary data to this article can be found online at http://dx.doi.org/10.1016/j.scriptamat.2016.10.028.

References

[1] B. Cantor, I.T.H. Chang, P Knight, A.J.B. Vincent, Mater. Sci. Eng. A 375 (2004) 213–218.
[2] J.W. Yeh, S.K. Chen, S.J. Lin, J.Y. Gan, T.S. Chin, T.T. Shun, C.H. Tsau, S.Y. Chang, Adv. Eng. Mater. 6 (2004) 299–303.
[3] S. Ranganathan, Curr. Sci. 85 (2003) 1404–1406.
[4] Y. Zhang, Y.J. Zhou, J.P. Lin, G.L. Chen, P.K. Liaw, Adv. Eng. Mater. 10 (2008) 534–538.
[5] B.S. Murty, J.-W. Yeh, S. Ranganathan, High-Entropy Alloys, 1st ed. Elsevier, 2014.
[6] M.C. Gao, J.-W. Yeh, P.K. Liaw, Y. Zhang, High-Entropy Alloys, Fundamentals and Applications, 1st ed. Springer, 2015.
[7] M. Niinomi, Biomaterials 24 (2003) 2673–2683.
[8] M. Niinomi, J. Mech. Behav. Biomed. Mater. 1 (2008) 30–42.
[9] T. Narushima, J. Jpn. Inst. Light Met. 55 (2005) 561–565.
[10] K. Hagihara, T. Nakano, H. Maki, Y. Umakoshi, M. Niinomi, Sci. Report. 6 (2016) 29779.
[11] A. Takeuchi, A. Inoue, Mater. Trans. 46 (2005) 2817–2829.
[12] S. Guo, Q. Hu, C. Ng, C.T. Liu, Intermetallics 41 (2013) 96–103.
[13] S. Fang, X. Xiao, L. Xia, W. Li, Y. Dong, J. Non-Cryst. Solids 321 (2003) 120–125.
[14] X. Yang, Y. Zhang, Mater. Chem. Phys. 132 (2012) 233–238.
[15] S. Guo, C. Ng, J. Lu, C.T. Liu, J. Appl. Phys. 109 (103505) (2011) 1–5.
[16] O.N. Senkov, J.M. Scotta, S.V. Senkova, D.B. Miracle, C.F. Woodward, J. Alloys Compd. 509 (2011) 6043–6048.
[17] O.N. Senkov, J.M. Scott, S.V. Senkova, F. Meisenkothen, D.B. Miracle, C.F. Woodward, J. Mater. Sci. 47 (2012) 4062–4074.
[18] See Sec. S2 in the Supplementary material
[19] M.G. Poletti, S. Branz, G. Fiore, B.A. Szost, W.A. Crichton, L. Battezzati, J. Alloys Compd. 655 (2016) 138–146.
[20] Y. Okazaki, Y. Ito, K. Kyo, T. Tateishi, Mater. Sci. Eng. A 213 (1996) 138–147.
[21] S.H. Lee, K. Hagihara, T. Nakano, Metall. Mater. Trans. A 43 (2012) 1588–1597.
[22] S.H. Lee, M. Todai, M. Tane, K. Hagihara, H. Nakajima, T. Nakano, J. Mech. Behav. Biomed. Mater. 14 (2012) 48–54.
[23] A. Chiba, K. Kumagai, N. Nomura, S. Miyakawa, Acta Mater. 55 (2007) 1309–1318.
[24] S. Hiromoto, E. Onodera, A. Chiba, K. Asami, T. Hanawa, Biomaterials 26 (2005) 4912–4923.
[25] L. Vegard, Z. Phys. 5 (1921) 17–26.
[26] M. Niinomi, Sci. Technol. Adv. Mater. 4 (2003) 445–454.
[27] X. Zhao, M. Niinomi, M. Nakai, J. Hieda, T. Ishimoto, T. Nakano, Acta Biomater. 8 (2012) 2392–2400.
[28] X. Zhao, M. Niinomi, M. Nakai, T. Ishimoto, T. Nakano, Mater. Sci. Eng. C 31 (2011) 1436–1444.